Stabilization and Characterization of Iron Oxide Superparamagnetic Core-Shell Nanoparticles for Biomedical Applications

12

Erik Reimhult and Esther Amstad

Keywords
Colloidal stability • MRI • NP • PEG • Polymer grafting • SPION • Surface functionalization

Introduction

Superparamagnetic iron oxide NPs, with core diameters between 3 and 15 nm, are used in a rapidly expanding number of research and practical applications in the biomedical field; the most common includes magnetic cell labeling [1, 2], separation [3], and tracking [3], for therapeutic purposes in hyperthermia [4, 5] and drug delivery [6] and for diagnostic purposes most prominently as contrast agents for magnetic resonance imaging (MRI) [7–9]. There are also many applications for smart hybrid materials functionalized with nanoparticle constituents for which superparamagnetic nanoparticles are an interesting alternative to provide a built-in actuator for heating or mechanical movement on the nanoscale.

Magnetic materials such as Co generally have higher saturation magnetization (M_s) than iron oxide [10] and would therefore serve as more efficient magnetic transducers or sensors. Biomedical applications are, however, constrained by the need for low toxicity and for regulatory approval. Iron oxide nanoparticles have a decisive advantage for biomedical applications [11], since they dissolve in a mild

E. Reimhult (✉)
Department of Nanobiotechnology, Institute for Biologically Inspired Materials, University of Natural Resources and Life Sciences Vienna, Vienna, Austria
e-mail: erik.reimhult@boku.ac.at

E. Amstad
Department of Physics, School of Engineering and Applied Sciences, Harvard University, Cambridge, MA, USA
e-mail: esther.amstad@seas.harvard.edu

B. Bhushan et al. (eds.), *Handbook of Nanomaterials Properties*,
DOI 10.1007/978-3-642-31107-9_19,

acidic environment found, for instance, in lysosomes. The resulting Fe^{3+} ions can be fed into the natural iron storage, which is 3–5 g of iron for an adult human [12, 13]. Thus, the additional amount of iron released from dissolved iron oxide NPs is negligible if iron oxide NP concentrations in the μg/kg body weight range are injected [14].

To allow dispersion of NPs in a matrix or liquid, especially in aqueous media and at physiologic salt concentrations, the common strategy is to surround the NP core with an organic polymer shell of so-called dispersants. NPs without a dispersant shell will rapidly aggregate through strong, mainly dipolar, interactions with themselves and with other molecules in solution. The presence of polymeric biomolecules such as proteins and saccharides with diverse surface physicochemical properties, ubiquitous in biological environments, strongly drives agglomeration and precipitation of clusters of nanoparticles through surface adsorption, bridging, and depletion interactions. The dispersant shell of NPs in biomedical applications not only prevents the direct aggregation of the NPs but also screens all interactions of the nanoparticle core with the biological molecules present in the environment that indirectly can induce agglomeration.

Commercially available superparamagnetic iron oxide NPs intended for magnetic labeling, cell separation purposes, and as MR contrast agents are typically stabilized with sugars such as dextran or synthetic polymers such as silicone [15]. These polymers used with molecular weights >10 kDa have a moderate affinity to the NP surface [16]. The resulting shell consisting of flexible polymers prevents NP cores from close interactions with other particles and proteins. This requires polymers to bind to the particle core, to be highly hydrated, and to induce repulsive interactions with proteins and other biomolecules. Due to the moderate affinity to iron oxide of these high molecular weight dispersants and the lack of a defined anchoring group, they often enwrap and cluster multiple iron oxide NP cores by direct physisorption to multiple NP surfaces. This results in poor control over cluster size (Fig. 12.1a) [17–20]. Furthermore, the dynamic rearrangement of the polymer shell results in a constantly changing interface of the nanoparticle.

An alternative strategy to disperse particles is to use a dispersant shell with low M_w (<10 kDa) where the polymer spacers are covalently bound to the nanoparticle core using an anchor that has high affinity for the NP surface (Fig. 12.1b). The anchors covalently linked to one end of the polymer chain assure an orientation of the polymer spacer and allow the use of polymer spacers with freely chosen properties, such as maximum hydration and protein repulsion, since the requirement to bind to the nanoparticle core can be relaxed. Using only one or closely spaced anchor groups ensures that these dispersants can bind to one NP core only. The resulting core-shell NPs can thus be divided into four components: the core, the anchor, the spacer, and optional surface functionalities (Fig. 12.1b). Each of these components can independently be adjusted through the modular buildup and defined geometry, rendering such NPs very versatile for a multitude of applications [21]. An important advantage resulting from the modular and controlled buildup is that the hydrodynamic size of the NPs can be precisely controlled, which

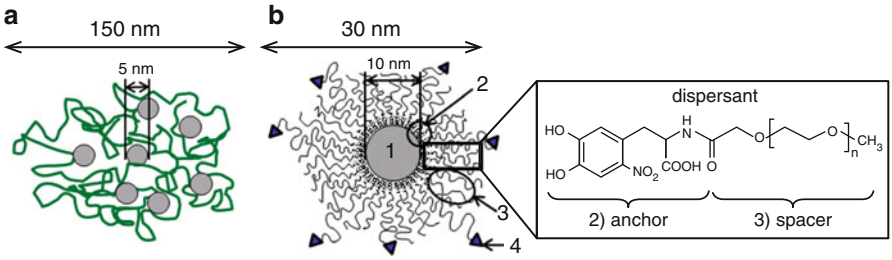

Fig. 12.1 Steric stabilization of iron oxide NPs. (**a**) Schematic of commercially available iron oxide-based MR contrast agents such as Feridex and Endorem. Superparamagnetic iron oxide NPs are coated with physisorbed high molecular weight dispersants such as dextran. The poor binding affinity of dextran leads to its reversible adsorption on the iron oxide NP surface. Furthermore, multiple iron oxide cores are embedded in one cluster. The resulting hydrodynamic diameter is many times larger than the core diameter. (**b**) Superparamagnetic iron oxide NPs stabilized with low M_w dispersants result in core-shell iron oxide NPs. These NPs can be divided into four components, namely, (*1*) core, (*2*) anchors, (*3*) spacers, and optionally (*4*) functionalities

is in contrast to NPs with dispersant shells consisting of physisorbed high M_w polymers. Furthermore, the well-defined assembly of dispersants at the NP surface enables controlled surface presentation of functionalities.

The size of NPs, their stability, dispersant shell thickness, and control over functionalities presented at the NP surface are the factors that determine NP performance in the demanding environment of a biological fluid [22, 23]. The structure of the dispersant shell which is determined by how it is assembled or synthesized will therefore control the performance of the NPs for their biomedical applications. An understanding of the influence of the type and assembly of dispersants on the NP surface and development of new types of dispersants are thus of pivotal importance for improving the performance of next-generation superparamagnetic NPs for imaging, drug delivery, and other demanding applications in biological fluids.

This chapter describes different aspects of NP stability, from its practical definition to its implementation. One goal is to link the understanding of the requirements on the molecular and nanoscale structure to different techniques by which they can be realized and to discuss their respective pros and cons. A critical point in nanoparticle research that is often not sufficiently appreciated in research focused on the clinical application of NPs is the challenge to characterize their actual physicochemical properties and structure. This includes the characterization of nanomaterials in an aqueous environment where most standard high-resolution imaging and chemical characterization techniques require specialized and demanding sample preparations. The definition and investigation of the colloidal stability of NPs might appear simple, but we will argue that it requires a comprehensive set of complementary characterization techniques. A careful reading of the literature also reveals that the meaning of stability

often varies from one paper to another and possibly from one subfield to another. We therefore also discuss the de facto definitions of NP stability to be found in the literature. After these general aspects, we describe how superparamagnetic iron oxide NPs are modified with dispersants of low and high surface affinity and M_w. Special attention is given to the selection of binding groups to tether the dispersants to the nanoparticle core, so-called anchors. This special attention is merited by the importance of anchors for the stability of the controlled surface modification. The synthesis of magnetic nanoparticle cores is treated in ▶ Chap. 7, "Magnetite and Other Fe-Oxide Nanoparticles," by Chiolerio et al. and will therefore not be discussed in this chapter. After establishing the different approaches to steric stabilization, we detail how dispersants have been optimized to gain close control over iron oxide NP stability, size, and functionalities by independently considering the influences of anchors and spacers. We also provide insights into the influence of the stability of superparamagnetic iron oxide NPs, and therefore the strategy for the stabilization and functionalization of iron oxide NP, on their magnetic properties. For a thorough review on the application of magnetic nanoparticles in the biomedical field, we refer to ▶ Chap. 15, "Magnetic Nanoparticles for Biomedical Applications," by Rivas et al., which complements the description of the design procedure of superparamagnetic nanoparticles in this chapter.

Characterization of Nanoparticles

Thorough characterization is essential to closely control the assembly of dispersants on the NP surface and to understand its influence on the size distribution, stability, and functionality of NPs. The optimal NP design can only be achieved if the detailed structure of the core-shell NPs is known in addition to the identification and quantification of the core-shell NP constituents. This is a challenging task given that the NP core and the dispersants used to encapsulate it are of similar size, but the methods used to characterize nanoscale inorganic particles and polymers are by necessity different and not always compatible. In practice we seek information on polymer shell thickness, polymer packing density, core size distribution, core morphology, and core surface roughness. We want to relate these properties to the assembly of dispersants into the shell and ultimately to NP colloidal stability in the biological environment and to presentation of functionality and functional groups.

The core size, size distribution, and morphology can be characterized with a combination of different techniques such as transmission electron microscopy (TEM) [24], X-ray diffraction (XRD) [24], and scattering techniques such as small-angle X-ray scattering (SAXS) [25] and small-angle neutron scattering (SANS) [26, 27]. The hydrodynamic diameter of dispersed NPs is defined as the effective diameter of the NP when diffusing in water; it is typically understood as the sum of the core diameter and twice the shell thickness. It can be assessed with scattering techniques, e.g., dynamic and static light scattering (DLS and SLS) [28], SANS [27], and X-ray disc centrifugation (XDC) [29].

The packing density of dispersants can be quantified with thermogravimetry analysis (TGA) [21, 30] and SANS [27]. To verify that only dispersants are adsorbed on the NP surface rather than impurities or capping agents such as oleic acid, and thus to assign the mass loss measured with TGA to the dispersants adsorbed on the NP surface, the chemical composition of stabilized NPs must be analyzed; this can be done with different techniques such as Fourier transform infrared (FTIR) spectroscopy [30, 31] or less common with X-ray photoelectron spectroscopy (XPS) [21]. To extract information about the packing density and density profile of dispersants from SANS results, it is highly beneficial to do contrast variation experiments, where the contrast of the core and shell are varied by changing the ratio of protonated to deuterated solvents and thus varying the scattering length density of the solvent [32]. Alternatively, information about the packing density of dispersants on the surfaces of NPs can be extracted from SANS results acquired with polarized neutrons [27]. Furthermore, the dispersant density profile can be assessed with SANS measurements [33].

Because of the different advantages and disadvantages of each characterization technique, it is highly beneficial to characterize NPs with multiple, complementary methods. However, attention has to be paid to the precise meaning of the results if results obtained with different methods are compared. Differences and artifacts can be introduced, for example, through different weighting of sizes, model-dependent extraction of parameters, and sample preparation protocols. Such aspects can lead to substantial differences in the quantification of a physical property of the NPs with different techniques.

Scattering techniques reveal intensity-weighted averages ($I(q) \propto r^6$) and are thus sensitive to the presence of large NPs and clusters in a sample. X-ray diffraction (XRD) reveals volume-weighted averages ($\propto r^3$), while TEM allows direct visualization of number-weighted ($\propto r$) structures. A comparison between TEM results and scattering data even for only slightly polydisperse samples can therefore yield a discrepancy that is created by the different intrinsic weighting functions if the weighting is not explicitly taken into account. The unskewing of the weighting is however only possible if the core size distribution is known. Scattering data are therefore more sensitive to the presence of even small proportion of aggregates and yield larger average sizes.

TEM reveals direct and at first glance model-independent information. Preparation of NP samples for TEM is done through drying on, e.g., carbon-supported TEM grids, unless TEM samples are prepared with cryo-preparation techniques. Drying of NP dispersions can introduce artifacts such as NP agglomeration and inhomogeneous assembly of NPs of different sizes. Furthermore, it leads to collapse of the dispersant layer that makes it impossible to accurately determine the thickness of the wet shell even if the coating can be visualized with TEM [34]. A complication with interpreting TEM data is that the apparent simplicity of measuring sizes from an image can obscure the fact that a choice of size is performed on the basis of image contrast. Instead of judging by eye, which often produces biased and arbitrary choices, an algorithm can be

applied that makes consistent choices of particle size based on image contrast and also allows automated image analysis to collect better statistics. In addition, such image analysis tools, like the freely available Pebbles [35], can improve the determination of the size beyond the direct image contrast by using knowledge of the particle symmetry to fit the grayscale image. NPs analyzed with this algorithm are slightly larger than they appear for most people doing the same measurement by eye. Despite the introduction of a model to interpret the data, automated analysis of TEM images retains the advantage that particle sizes and histograms are compiled on the single particle level.

Scattering techniques allow analyzing NPs directly in dispersion and are therefore less prone to sample preparation artifacts and better suited to determine the thicknesses of the shell. However, they require model-dependent data analysis that is performed on the entire ensemble. SANS and SAXS data are fitted with form factors and, if required by particle-particle interactions, with superimposed structure factors. The form factors assume a certain structure and size distribution of the evaluated objects. Therefore, accurately done, the data analysis requires detailed prior knowledge about the shape and structure of the analyzed objects. If the quality of the scattering data is sufficient, the dispersant shell density profile can be obtained by comparing scattering data to a set of models. However, the concentration of NPs can critically affect the outcome of scattering results. If the concentration of NPs is high, multiple scattering produces severe artifacts in light scattering results [36]. SANS and SAXS data acquired on highly concentrated NP dispersions typically include a structure factor contribution that is convoluted with the form factor [37]. While the form factor describes the size distribution and shape of NPs, the structure factor is influenced by inter-particle interactions, clustering, and assembly of NPs. Because multiple scattering and structure factor contributions can significantly influence scattering results, it is very important to prepare samples such that effects of the NP concentration on the scattering results can be excluded or appropriately accounted for. The low scattering signal obtained from dilute core-shell particle samples, which mainly comprise weakly scattering, highly hydrated polymer shells, requires very long data acquisition times to obtain high-resolution data. This is seldom possible due to the restrictions on the facilities that can acquire SANS and SAXS data; a detailed experimental determination of the shell structure is therefore elusive.

Dynamic light scattering using commercial benchtop instruments is often applied to determine the hydrodynamic size of core-shell NPs in solution. DLS does not directly analyze the scattering of the particle to obtain its structure, but instead the time-correlation of the scattering intensity which relates to the Brownian motion to the hydrodynamic size of the NPs. The commercial versions of this method are best suited for dilute samples of strongly scattering objects with sizes in the 100 nm range. The NPs to be analyzed should be homogeneous and absorb neither light nor fluoresce. Unfortunately, magnetic nanoparticles and in particular iron oxide nanoparticles strongly absorb light; this compromises the reliability of DLS size measurements. Qualitatively it might be used to track changes in aggregation using the scattering intensity, which is sensitive to the size, as well as

the hydrodynamic size to assess the colloidal stability of the nanoparticle dispersion. This is particularly useful to assess the influence of external parameters, such as a change in temperature, on the stability of NPs [21].

The fact that the analysis of data acquired with scattering techniques is model dependent renders a comparison to data acquired with complementary, model-independent, or less model-sensitive techniques highly advantageous. The comparison of the quantification of NP parameters obtained using scattering techniques with quantification measured with model-independent techniques allows checking the validity of the model assumed to analyze scattering data.

The value of characterizing NPs with different, complementary techniques can be exemplified by the determination of the packing density of dispersants and their density profile. These parameters can be measured and quantified with SANS. However, to analyze SANS data, a form factor that comprises assumptions about the core-shell structure of the NPs including the dispersant density profile has to be applied to analyze the scattering data.

The ratio of the mass of organic to inorganic materials can be quantified with TGA, although no information on the density profile can be obtained. To ensure that the mass loss of organic molecules measured with TGA can exclusively be assigned to dispersants rather than to impurities or remaining capping agents, further chemical analysis on the stabilized NPs such as FTIR or XPS is required [21]. However, also after excluding the influences of impurities, the determination of dispersant grafting density by TGA is very sensitive to assumptions and further input data. The determination of the grafting density requires normalizing the measured ratio of organic to inorganic mass to the surface area of the NPs, using a distribution of the molecular weight of the dispersant. The surface area of the nanoparticles is only known if the size distribution of the cores is known. Since the surface-to-volume ratio of nanoparticles is very high, even small errors in the size distribution of NP cores propagate to large uncertainties in the grafting density. Furthermore, this normalization is almost always performed for assumed smooth and spherical cores. Depending on the synthesis method, the cores can have highly irregular, faceted, or rough morphologies; the surface area of NP cores is therefore often underestimated. Also, the poor statistics obtained from TEM images does not allow for an accurate assessment of the size distribution of the cores in a scattering sample as described above. This information must be obtained iteratively by fitting scattering data with form factors that agree with the shape and morphology of NPs seen in TEM images. Therefore, the dispersant packing density and density profile on NPs can only be revealed if NPs are characterized with multiple methods, such as SANS, TGA, TEM, and FTIR spectroscopy in concert.

Nanoparticle Stability

NPs are stable if the inter-particle potential (U_{tot}) has an energy barrier that is high compared to k_BT. In a first approximation, U_{tot} of NPs contains four contributions, the attractive van der Waals and magnetic potentials and the repulsive electrostatic

and steric potentials [38, 39]. These potentials can be calculated if the core radius, shell thickness, saturation magnetization, zeta potential, and dispersant density profile are known [38–40]. Considering the four main contributions to U_{tot}, NPs can be electrostatically or sterically stabilized. Optionally, the two stabilization methods can be combined. Electrostatic NP stabilization is only effective at low ion concentrations where the Debye screening length is on the order of tens of nm and at pHs far above or below the isoelectric point (IEP) of NPs. However, biomedical applications require good stability of NPs under high salt concentrations and over a range of pHs. The macromolecules, predominantly proteins, present in a biological fluid also contain both positively and negatively charged residues; typically they are zwitterionic and carry opposite charges in patches on the protein surface. To avoid interactions of NPs with these macromolecules, NPs must be sterically stabilized [41, 42] and the colloidal stability of the resulting core-shell NPs has to be evaluated for biomedical applications.

The interaction potentials of NPs cannot be measured directly due to the limited resolution of the techniques developed for such investigations on microparticles. Hence, in practice, the term 'stability' has been used with very different meaning in the literature on NPs, mostly without explicit acknowledgment of these differences. NPs are often considered stable if they do not visibly precipitate over a finite period of time [43, 44]. A thorough characterization of NP dispersions, e.g., with scattering techniques allows to define NP stability more precisely.

The importance of the technique and conditions used to characterize NP stability was exemplified on poly(ethylene glycol)-hydroxydopamine (PEG-hydroxydopamine)-stabilized superparamagnetic iron oxide NPs. PEG (0.55 kDa)-hydroxydopamine-stabilized iron oxide NPs were stable for more than a year if stored dispersed and analyzed at RT [21]. However, PEG (5 kDa)-hydroxydopamine-stabilized iron oxide NPs agglomerated if they were subjected to multiple filtrations (Fig. 12.2) [21]. If dispersants adsorb reversibly at the NP surface, dispersants adsorbed on the NP surface are in equilibrium with unbound dispersants in solution. If NP dispersions are filtered, free dispersants are removed. To reestablish the equilibrium in the NP dispersion, some dispersants adsorbed at the NP surface desorb, leading to a lower dispersant packing density at the NP surface. The dispersant packing density at the NP surface decreases with increasing number of filtration steps. If the dispersant packing density at the NP surface drops below a critical value, NPs start to agglomerate [45]. The fact that PEG (5 kDa)-hydroxydopamine-stabilized iron oxide NPs agglomerated after filtration indicates that hydroxydopamine adsorbs reversibly on Fe_3O_4 surfaces. However, if the dispersant packing density at the NP surface is sufficiently high under the conditions NP dispersions are stored, then NPs remain long term stable even if they are stabilized with reversibly binding anchors such as hydroxydopamine.

Applications of superparamagnetic iron oxide NPs in vitro in cell cultures and in vivo always include high dilutions of NP dispersions. Therefore, reversible dispersant adsorption that leads to agglomeration of iron oxide NPs can have severe adverse consequences for these applications. Once injected into a living

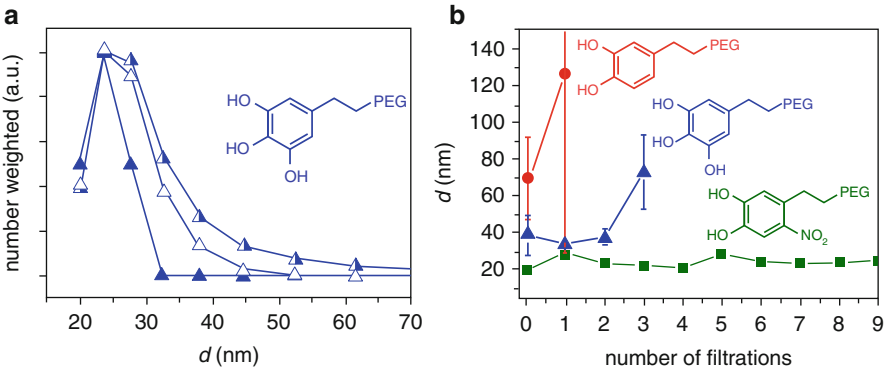

Fig. 12.2 Characterization of the stability of superparamagnetic iron oxide NPs. The stability of superparamagnetic iron oxide NPs was measured with DLS at 25 °C. (**a**) The hydrodynamic diameter of PEG (0.55 kDa)-hydroxydopamine stabilized iron oxide NPs as-stabilized (-▲-), after storage for 1 year in PBS (-◭-) and after storing them for 20 months in HEPES (-△-).[21] (Copyright Wiley-VCH Verlag GmbH & Co. KGaA. Reproduced with permission). (**b**) The stability of superparamagnetic iron oxide NPs was evaluated as a function of the number of filtrations performed to remove excessive dispersants of iron oxide NPs stabilized with PEG (5 kDa)-nitrodopamine (-■-), PEG(5 kDa)-hydroxydopamine (-▲-), and PEG (5 kDa)-dopamine (-●-). [21] (Nano letters by American Chemical Society. Reproduced with permission of AMERICAN CHEMICAL SOCIETY in the format Journal via Copyright Clearance Center) While PEG-hydroxydopamine stabilized iron oxide NPs were stable at RT for more than 20 months, they started to agglomerate after excessive dispersants were removed by more than two filtrations. This indicates that superparamagnetic iron oxide NPs agglomerate upon dilution and will lead to adverse consequences if applied in vivo

body, agglomeration of NPs is difficult to assess because the size of NPs can no longer be measured. Additionally, once NPs are exposed to cells or injected into the body, agglomeration of NPs is convoluted with other effects such as exposure to many different proteins that might adsorb to the NPs or even displace reversibly anchored dispersants. The result is a poorly defined system. An accurate analysis of this system such as a study of the efficiency of targeting NPs to desired locations by the addition of ligands to the NP shell is difficult. The effects caused by engineering the surface of core-shell NPs are convoluted with effects caused by uncontrolled NP agglomeration and nonspecific protein adsorption on the NP surface. This illustrates the necessity to characterize NPs stringently, especially if they are intended for biomedical applications. Thus, also for NPs that are shown colloidally stable under dilute conditions with the dispersants remaining tethered to the core, the in vivo colloidal stability must be assessed by studying the NP tendency to aggregate in dilute solutions of serum or cell media. It is particularly important to understand the colloidal stability in serum where sticky macromolecules are present, which can compete with the dispersants for access to the core surface and, if adsorbed to the NP, induce a cascade of interactions from nonspecific bridging of particles to signaling and opsonization.

Steric Stabilization of Iron Oxide Nanoparticles Using Polymer Shells

Nanoparticles that have to be stable in aqueous media containing high concentrations of ions must be sterically stabilized [41, 42]. Steric stabilization relies on polymers, so-called dispersants, which surround NP cores. Dispersants with a high affinity to the solvent they are dissolved in provide a sufficiently thick shell around the NP core to overcome the attractive van der Waals and magnetic potentials. They therefore impart long-term colloidal stability under dilute conditions, at high salt concentrations, and at elevated temperatures. Dispersants used to sterically stabilize superparamagnetic iron oxide NPs can be divided into two groups. One group of dispersants are high molecular weight polymers consisting of repeat units that have a low affinity to the surface of iron oxide NPs. This leads to reversible adsorption of the dispersant. The other group of dispersants typically consists of a high affinity anchor that is covalently linked to a low molecular weight (M_w) spacer, usually below 10 kDa.

Physisorption of High M_w Dispersants

Superparamagnetic iron oxide NPs used for clinical applications are currently most often coated with high M_w polymers such as dextran [46], alginate [47], chitosan [48], poly(vinyl amine) (PVA) [49–51] or poly(acrylic acid) (PAA) [52], or by electrostatically adsorbing charged polymers like poly(ethylene imine) (PEI) to which subsequently a layer of poly(ethylene oxide)-*b*-poly(glutamic acid) (PEO-PGA) can be adsorbed [53]. These polymers lack a well-defined high affinity anchor that irreversibly bind them to the surface of iron oxide NPs and typically have a molecular weight >10 kDa [9]. Therefore, such dispersants often encapsulate multiple cores within one cluster, and the resulting hydrodynamic cluster radius is many times larger than the radius of individual cores [18–20]. The weak physisorption of the stabilizing polymer dispersants compromises iron oxide NP stability [54], leads to protein adsorption onto the core particle, and drastically decreases blood circulation time if applied in vivo [55]. The poorly defined interface of such NPs also prevents controlled functionalization in terms of number and presentation of ligands [54].

One solution to this problem is to cross-link the enwrapping polymer [56]. However, this renders control over the thickness of the dispersant layer difficult, and the resulting hydrodynamic diameter was much larger than that of single cores [56]. Additionally, epichlorohydrin, the cross-linking agent used to cross-link the dextran in these studies, is classified as cancerogenic, mutagenic, and reproxotic [57, 58], which could limit its clinical use.

Grafting of Low M_w Dispersants

An attractive approach to obtain core-shell NPs with control over size, interfacial stability, and the presentation of functional groups at the surface in a defined manner is to use low M_w dispersants that consist of one well-defined anchor covalently linked to a spacer polymer (Fig. 12.1b). Low M_w dispersants can be bound to NP surfaces either through the 'grafting to' or the 'grafting from' technique (Fig. 12.3). For the latter approach, initiators are covalently bound to the NP surface. Spacers can subsequently be grown in situ, by different polymerization routes, such as through radical polymerization (Fig. 12.3a) [59, 60]. The grafting density of dispersants is determined by the density of anchors with initiator groups at the NP surface. This results in a highest packing density of dispersants and excellent NP stability.

Although the 'grafting from' technique results in a high packing density of dispersants, it has some inherent drawbacks. The characterization of dispersants and control over the dispersant polydispersity and the shell thickness are difficult, despite that the use of living polymerization should ensure excellent control over chain length. Controlled polymerization is difficult to scale up to large volumes and in the presence of high concentrations of nanoparticles, which might affect the polymerization conditions. Furthermore, functionalization of stabilized NPs with different ligands or other functional units and controlling the density of functional groups presented at the NP interface are challenging [61].

Low M_w dispersants synthesized prior to their adsorption on the NP surface can be characterized with conventional chemical characterization methods. They can be grafted to the NP surface without performing in situ chemistry by using suitable anchors (Fig. 12.3b). This self-assembly approach has the advantage that it is cost-effective, has high reproducibility, and is easy to scale up. The thickness of the dispersant layer can be controlled by the spacer configuration, packing density, and M_w of the dispersant. The density of one or multiple ligands presented at the surface can be tailored by co-adsorbing differently functionalized dispersants in one or several subsequent assembly steps [21, 62]. Polymers adsorbed through the 'grafting to' approach pack at a significantly lower density on flat surfaces than the polymers adsorbed through the 'grafting from' approach [61]. This difference is a result of that steric repulsion of dispersants already adsorbed on surfaces; it hinders the grafting of additional dispersants and thus limits the maximum grafting density. By contrast, the maximum packing density of dispersants using 'grafting from' the surface is limited only by the footprint of the anchor [63, 64]. At a highly curved interface of a NP, the lateral steric repulsion of grafted polymers is reduced due to the rapidly increasing free volume available to dispersants with increasing distance from the core. Therefore, the difference in grafting densities of surfaces modified through the 'grafting from' and the 'grafting to' approaches is expected to decrease with increasing surface curvature (Fig. 12.4). However, it still limits the maximum M_w of dispersants that can be grafted to the surface at a given packing density.

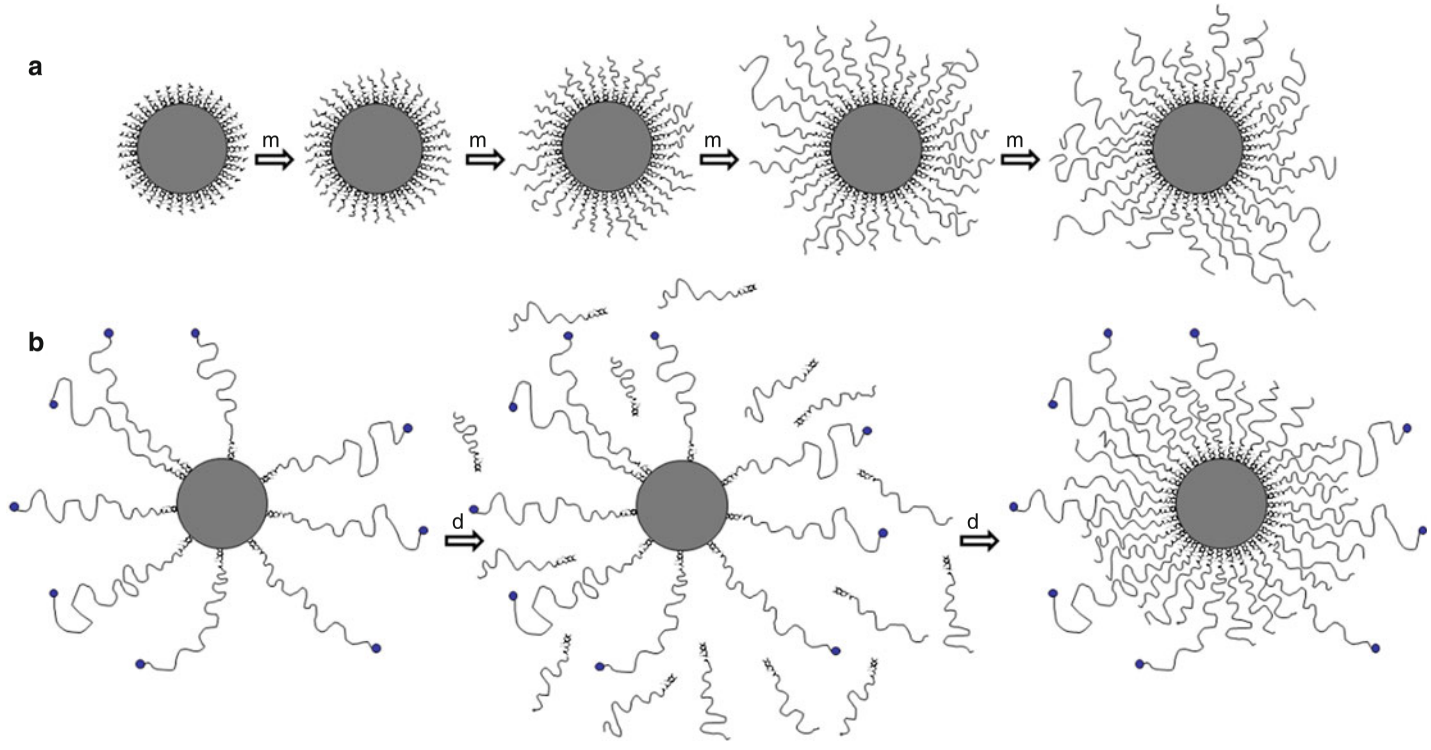

Fig. 12.3 Modifying iron oxide NP surfaces with low M_w dispersants. Low M_w dispersants can be (**a**) grafted from and (**b**) grafted to the NP surface. If low M_w dispersants are grafted from the NP surfaces, initiators are firmly bound to the NP surface. After monomers (m) were added to the NP dispersion, dispersants are grown in situ, typically through a radically initiated chemical reaction. Dispersants grown in situ are densely packed on the NP surface; however, control over the length of dispersants, their polydispersity, and density of functionalities presented at the NP surface is difficult. Alternatively,

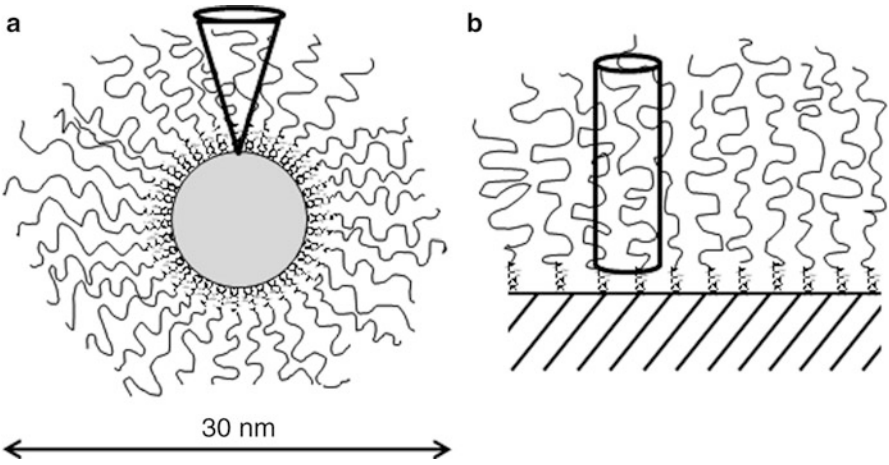

Fig. 12.4 Free volume of dispersants. The free volume of dispersants adsorbed on (**a**) NPs and (**b**) flat surfaces. While the free volume of dispersants adsorbed on NPs increases conically with increasing distance to the NP surface, it remains constant for dispersants adsorbed on planar surfaces

Anchors

Low M_w dispersants have to firmly adhere to the NP surface through suitable anchors (Fig. 12.1b). Ideally, the binding affinity of anchors is high and its desorption rate k_{off} negligible. Naturally, anchors that meet these stringent requirements can be used both to immobilize initiators for 'grafting from' polymerization of dispersants and to graft polymer brushes to a NP surface. Typical anchors to modify surfaces of superparamagnetic iron oxide NPs described in the literature are catechol [65–68] or catechol derivatives [21, 69, 70], carboxy groups [71–73], phosphonates [72, 74, 75], and silanes [76–80].

Despite the importance of anchors for the NP stability and to define the density of functional units on a NP, the influence of the affinity of anchors to NPs has only been studied recently. Similar catechol anchor chemistries were shown to result in large variations in affinity to iron oxide; this translated into large differences in colloidal stability of superparamagnetic Fe_3O_4 NPs stabilized by low M_w PEG-based dispersants [21]. Due to the lack of characterization of anchor stability, only a few irreversibly binding anchors have been identified. The bulk of the

Fig. 12.3 (continued) dispersants (d) are synthesized prior to the adsorption on the NP surface. These dispersants are grafted to the NP surface. The resulting packing density of dispersants is lower than that of dispersants grafted from the surface of NPs. However, the grafting to approach allows for close control over the thickness of the dispersant shell and the density of functionalities presented at the NP surface. The latter is achieved by adsorbing a defined concentration of functionalized dispersants at the NP surface. The NP surface is subsequently backfilled with non-functionalized dispersants

literature on superparamagnetic iron oxide NP contrast agents thus uses NPs stabilized with *reversibly* binding dispersants, which often implies compromised colloidal stability.

Messersmith and coworkers demonstrated that the affinity of reversibly binding anchors can be significantly improved by designing multivalent anchors; they achieved high densities of polymer brushes that were grafted to flat surfaces [81]. The enhanced binding affinity could only be observed if the multiple binding groups were interconnected by sufficiently flexible linkers [81]; longer flexible linkers would be required to achieve the same improvement in binding affinity on the highly curved surface of a NP. The surface area occupied by multiple anchors is considerably larger than that of a single anchor, which might critically decrease the packing density of dispersants on highly curved surfaces. On these surfaces, the density of anchors might limit the maximum packing density of dispersants as the lateral steric repulsion of adjacent spacers is considerably lower than on flat surfaces [82].

Among the commonly described anchors, phosphonic acid has been reported to be too weak to replace carboxy groups from iron oxide NP surfaces [83]. Furthermore, carboxy groups were shown to be replaced by proteins [84] and compared unfavorably to catechols and nitrocatechols [21]. Silanes pose experimental difficulties in the assembly of dispersants on the surface of iron oxide NPs as they have to be adsorbed in water-free solvents, but anchor hygroscopic polymer spacers. Furthermore, they can cross-link which compromises the control over the assembly of silane anchored dispersants [85].

Inspired by the presence of catechols in organisms for fixation of metals and for surface adhesion, superparamagnetic iron oxide NPs have increasingly been surface modified using this chemical motif [86]. Because of the biological relevance of DOPA/Fe^{3+} and dopamine/Fe^{3+} complexes, their structure [87–89] and electronic interactions [90, 91] have been studied in detail. Despite their recent popularity, their suitability as anchors to stabilize iron oxide NPs is debated. Iron is well known to catalyze catechol oxidation leading to semiquinones, quinones, and eventually carboxy-containing products [92–94]. Oxidative degeneration of dopamine adsorbed on iron oxide NPs that results in a loss of the stability of NPs has also been reported [95], and recently, cryo-TEM images of PEG-dopamine stabilized Fe_3O_4 NPs revealed their agglomeration [96].

Already in 1976, it was noticed that electronegative substituents on the catechol ring strengthen the iron-catechol bond. The bond of nitrogen-substituted catechols (nitrocatechols) to iron ions remained unchanged for 24 h at 25 °C [97]; this is considered an irreversible bond. It was speculated that nitrocatechols can act as oxidizing agents which was assumed to be the reason for this exceptionally strong bond [97]. Detailed studies on the binding of nitrocatechols to iron ions revealed a significantly lower tendency to generate radicals for nitrocatechol/iron compared to catechol/iron complexes [98]. Based on complexation studies of these anchors with Fe^{3+}, the increased complexation strength of electronegatively substituted catechols compared to unsubstituted counterparts was related to the increased acidity of the former compounds [99, 100]. Recently, electron paramagnetic

resonance (EPR) studies on superparamagnetic iron oxide NPs coated with nitroDOPA revealed an enhanced electron density at nitroDOPA anchors and electron-depleted iron ions on the NP surface [70, 101]. To the contrary, dopamine is known to oxidize if adsorbed to iron oxide surfaces [95].

The strong complexation of nitrocatechols to Fe^{3+} ions and enhanced electron density at the nitroDOPA anchors have been shown to directly relate to the high stability of grafted polymer films when nitrocatechols are used as anchors. The stability of superparamagnetic iron oxide NPs with shells of PEG-nitroDOPA or PEG-nitrodopamine was shown to be much higher than that of iron oxide NPs stabilized with PEG-DOPA and PEG-dopamine [21]. Follow-up studies revealed that the binding affinity of anchors to the metal ion of oxides has to be optimized rather than maximized to achieve good stability of iron oxide NPs [70, 102], since the anchor with the highest binding affinity resulted in dissolution of the iron oxide cores.

Spacers

The spacer part of a dispersant (Fig. 12.1b) has to prevent that the NPs get into sufficient proximity for the van der Waals and magnetic interactions to dominate. If two sterically stabilized cores approach each other, the volumes of the respective polymer shells are confined. This reduces the entropy of dispersants and increases the osmotic pressure between NPs. The resulting repulsive potential critically depends on the density profile of dispersants, their packing density [103], binding reversibility, and the solvent quality with respect to the dispersants [104]. The design and optimization of sterically stabilized core-shell NPs would be greatly facilitated if these parameters were known. Only then can the inter-particle potentials be calculated [105, 106]. Recent theoretical investigations of density profiles of dispersants adsorbed on surfaces of NPs have been performed with models that are sufficiently similar to the relevant application examples to serve as a guide to further optimize core-shell NPs.

Polymer Density Profiles on Highly Curved Surfaces

The standard theories to study spherical brushes, i.e. brushes from interfaces that are curved on the length scale of the spacer, build on the framework originally developed by Alexander and de Gennes for planar brushes [105, 107–109]. Refinements of scaling and self-consistent field (SCF) models [110] led to the finding that polymer density profiles change from parabolic to step function as the brush grafting density is increased.

Early attempts to apply scaling theory to NPs resulted in a dispersant density profile decaying exponentially with increasing distance from the surface of NPs [111]; this is clearly different from the parabolic decay obtained on flat surfaces [112]. These attempts however neglected that the scaling approach and

the Derjaguin approximation fail if the dimensions of the solvated dispersant chain approach or exceed the core diameter, which is the case for sterically stabilized superparamagnetic iron oxide NPs. Applying SCF calculations [113, 114] and Monte Carlo (MC) simulations [115] to chains grafted to a surface of NPs allows extraction of more detailed information and has resulted in a different, more parabolic-like density profile with the core interface region depleted by free polymer end segments [116].

The assumption of negligible interchain penetration inherent to the models described above only holds for long chains and low packing densities. Short chains significantly interpenetrate adjacent chains; this alters the dispersant density profile. Deviations from the parabolic polymer density profile are seen for polymer chains shorter than 1,000 repeat units; they result in an earlier and gradual onset of repulsive inter-particle forces compared to inter-particle potentials calculated for parabolic polymer density profiles [117]. Furthermore, the dispersant density profile was predicted to undergo a smooth change from a parabolic decay at low surface curvatures and for small or stiff dispersants to a power law decay similar to that of star polymers as the curvature increased relative to the length of the polymer spacer [104, 118]. Recently, very good agreement between the power law decay of the density profile for star polymers and relevant model NPs with high grafting densities of linear polymers was shown using density functional theory calculations and coarse-grained molecular dynamics simulations [119]. Increasing the chain length or grafting density resulted in an increasingly sharp cut-off of the region with power law dependence, as well as a smeared out distribution of the free-end segments. As chain interpenetration starts, the interaction potential is only a few k_BT; by contrast, a very strong repulsion is obtained as the particles get close due to the rapidly increasing polymer density [120].

In summary, the lack of experimental data to evaluate the contradictory theoretical findings has led to an ongoing debate about the density profile of polymers adsorbed on highly curved surfaces. The lack of experimental data is a result of a lack of experimental techniques that can investigate with sub-nm resolution the structure and interaction potentials of polymers grafted to nanoparticles. Compounding this problem is the lack of experimental data on dispersants *irreversibly* grafted to highly curved surfaces. Reversible adsorption of dispersants introduces time-dependent changes to the grafting density and density profile of dispersants. The best suited experimental methods to assess the shell density profile are scattering techniques such as SANS, but any free desorbed dispersant will scatter and smear the information on the shell density profile. Thus, there are very few experimental investigations which directly relate to the theoretical work. Experimentally, it has been demonstrated that the colloidal stability is decreased as the PEG M_w is decreased for similar grafting densities [70]. A direct comparison to density profiles was however not shown. Another interesting recent finding was that iron oxide NPs also could be functionalized by nitrocatechol-anchored PEG-dendrimers, which should provide a different dispersant density profile to the standard linear polymer surface modifications [121]. It was shown that NPs remained colloidally stable if the PEG-dendrimers were irreversibly bound to the

NP surface and were at least second generation. A dendrimer is compact and rigid but provides a much higher EG density close to the surface than a linear PEG chain; this might be the reason for the observed stability. However, the thin shell did not completely screen the surface charge of the core and anchor region [121, 122]. The resulting additional electric double layer repulsion contributes to colloidal stability under the measurement conditions but would be detrimental for applications in the biomedical field. However, the possibility to use dendritic spacers to make ultra-small iron oxide NPs with a high degree of controlled functionalization is a tantalizing prospect that warrants more theoretical and experimental attention.

Effect of Shell Properties on Protein Resistance and In Vivo Response

Superparamagnetic iron oxide NPs intended for biomedical applications have to be colloidally stable and to resist adsorption of biomacromolecules such as proteins, a property often referred to as 'stealth'. It is a necessity for their successful application in vivo. If plasma proteins such as opsonins are adsorbed on the surface of NPs, NPs are taken up by macrophages, monocytes, and dendritic cells and thus initiate their clearance [123]. The requirement of resistance to protein adsorption precludes electrostatic stabilization, because most proteins express multiple charged groups on their surface. As a result, NPs must be sterically stabilized with a polymer shell for which proteins and other biomolecules have no affinity.

The most commonly used dispersant spacer that renders NPs stealth is poly(ethylene glycol) (PEG) [12, 20]. PEG-modified surfaces exhibit extremely low attractive van der Waals forces compared to other well-known water-soluble polymers due to the low refractive index of PEG [124]. Furthermore, protein adsorption onto highly hydrated polymers such as PEG leads to confinement of the polymer chains; the entropy decrease renders this adsorption energetically unfavorable [125]. A final factor contributing to the protein repellency of PEG is the ordering of water around PEG chains [126]; this prevents direct contact of PEG with proteins [127]. However, PEG is known to be prone to degeneration if applied in vivo [128, 129]. Possible alternatives exist; in vitro studies showed that poly (2-methyl-2-oxazoline) (pMOXA) has similar protein-repelling properties to PEG but is far less prone to degradation [130].

Nanoparticles must be stabilized with irreversibly grafted dispersants to ensure that the resistance of NPs to protein adsorption is correctly evaluated. A physisorbed surface coating can be partially replaced by adsorbing proteins. Such processes have to be excluded as the evaluation of protein resistance is mainly done by tracking nanoparticle size and the mass fraction of organic materials, which both can be insensitive to dispersant replacement.

Protein adsorption has been studied in detail on PEG-modified planar surfaces where quantitative surface-sensitive characterization techniques such as XPS and time-of-flight secondary ion mass spectroscopy (ToF-SIMS) can be used to chemically verify the presence and surface coverage of proteins [81, 131, 132].

It was found that protein adsorption decreases almost linearly with increasing density of ethylene glycol (EG) monomers at the surface. For a surface to be protein resistant, the EG surface densities must be >15–30 nm^{-2} [81, 131]. The existence of a threshold value for the EG density to render surfaces protein resistant has direct consequences for the packing density and the M_w of the grafted PEG chains, as they both linearly affect the projected EG surface density. A high packing density of PEG is especially crucial to prevent adsorption of small proteins, while the adsorption of large proteins is less sensitive to it [132–135]. Generally, protein resistance requires that the grafted PEG chains are in the so-called brush regime, in which the distance between adjacent chains is smaller than the Flory radius of the polymers [107, 136].

The PEG M_w and EG surface density are crucial parameters for the protein resistance and thus circulation time of NPs, as could be expected from the results for planar surfaces. However, the critical EG density above which NPs are protein resistant might be higher on highly curved surfaces of NPs than it is on flat surfaces. The high surface curvature of a NP leads to a conically increasing free volume for the PEG spacer and possibly a polynomially decreasing polymer density [119] with increasing distance from the surface of the NP core (Fig. 12.4). Thus, if coated with the same grafting density and M_w of PEG, proteins can come much closer to surfaces of NPs than to flat surfaces. This was exemplified in a study, where protein resistance of 100 nm diameter poly(lactic acid) (PLA) NPs stabilized with PEG (2 kDa) could only be obtained if the PEG packing density was ≥0.2 molecules/nm^2 [137]. For lower PEG packing densities, circulation times increased with increasing M_w*s* of PEG due to an increased EG density [55]. Protein adsorption on 200 nm diameter PLA NPs could be significantly decreased if at least 5 wt% PEG (5 kDa) was added to the PLA NP surface [55]. At this concentration, PEG should be in the brush regime as the distance between two PEG chains was 1.4 nm [55], whereas the Flory radius of PEG (5 kDa) is 5.1 nm and the curvature of the core is rather low. However, due to steric repulsion and depending on the grafting method, the packing density of PEG might also decrease with increasing PEG M_w. A too low packing density of PEG in itself compromises the stability of NPs and sets an upper limit to the suitable M_w range [45]. Thus, grafting densities and M_w*s* of PEG chains cannot be directly substituted for each other. Due to these reasons, PEG M_w*s* in the range 1.9–5 kDa have been found optimal to disperse superparamagnetic iron oxide NPs intended for biomedical applications [70, 133, 138]. These NPs showed prolonged circulation times in vivo [139, 140].

Biodistribution: Relation to Nanoparticle Size and Stability

In addition to the surface chemistry, which determines the affinity of proteins to adsorb on NP surfaces, the fate of NPs in vivo is influenced by the size, shape [49, 141], and surface charge of NPs [142, 143]. While particles larger than 200 nm are rapidly cleared by the spleen, NPs smaller than 10–50 nm are generally removed from the body through extravasation and renal clearance [12, 57].

The optimal range of the hydrodynamic diameter for in vivo applications of intravenously injected NPs that require prolonged blood half-life times is therefore typically 10–100 nm.

Superparamagnetic iron oxide NPs stabilized with PEGylated dispersants and administered to nude mice have been reported to mainly end up in the liver and spleen if their size is 30–50 nm [144]. The clearance of PEGylated NPs was shown to depend on the affinity of the dispersant anchors to the NP surface [123, 145]. The circulation time was substantially prolonged for NPs stabilized with covalently attached compared to physisorbed PEG [55, 145]. The fast clearance of the latter NPs was assigned to the fact that proteins could replace physisorbed PEG; this results in an activation of clearing mechanisms.

Similar to PEG-stabilized superparamagnetic iron oxide NPs, dextran-coated, agglomerated iron oxide NPs accumulate in the liver and spleen. In addition to slow clearance and a tendency to agglomerate [146], NPs coated with dextran have also been shown to induce differentiation of monocytes into macrophages [54].

Effect of Shell Properties on Magnetic Properties

The magnitude of the magnetic response of a superparamagnetic iron oxide NP is determined by its saturation magnetization (M_s). The higher the saturation magnetization of superparamagnetic iron oxide NPs, the easier they can be magnetically separated and ferried to desired locations. A high M_s also locally induces a strong magnetic field gradient if a homogenous magnetic field is applied. The local perturbation of the magnetic field is responsible for the changed relaxivity, r_2, of surrounding water molecules measured in MRI. Thus, the higher the M_s of superparamagnetic iron oxide NPs, the more effective they are as magnetic resonance contrast agents [12].

The magnetic properties of NPs depend on the composition, size, and shape of their core [12]. However, M_s of superparamagnetic iron oxide NPs is always below that of the bulk material, and it decreases with decreasing size of the core [147]. This decrease has been assigned to surface anisotropy effects [148, 149], which become increasingly important as the surface-to-volume ratio increases with decreasing size of the NP cores.

Effect of Surface Modification on Saturation Magnetization of Superparamagnetic Iron Oxide Nanoparticles

The M_s has been shown to decrease if superparamagnetic iron oxide NPs are sterically stabilized [21, 150]. However, a direct comparison of stabilized and unstabilized superparamagnetic iron oxide NPs requires normalization of the M_s to the mass of iron oxide to account for the lower wt% of NP cores in NPs stabilized with dispersants compared to bare counterparts. The lower M_s of surface functionalized iron oxide NPs might be related to interactions of the anchors with

surface iron ions that influence the magnetism of the iron oxide NP surface layer [101, 102]. Therefore, improved stability of iron oxide NPs induced by irreversibly anchored dispersants might partially come at the expense of lower M_s values.

One common way to demonstrate good magnetic properties of stabilized superparamagnetic iron oxide NPs dispersed in solution is to show their attraction to a small tabletop magnet. However, individually stabilized superparamagnetic iron oxide NPs have too low M_s to be strongly attracted by a small tabletop magnet. In contrast, agglomerates are readily attracted by such magnets [21, 43]. Therefore, tests in which iron oxide NPs are rapidly cleared from aqueous solutions using tabletop magnets not only indicate good magnetization of the superparamagnetic iron oxide NPs but also poor NP stability.

Relaxivity

Superparamagnetic iron oxide NPs enhance contrast in MR images by changing the relaxation times r_1 and r_2 of adjacent water molecules [12]. The exchange rate of water molecules in the first hydration shell of superparamagnetic iron oxide NPs mainly determines r_1. Thus, r_1 depends on the accessibility of water molecules to the iron oxide core surface. Commercially available superparamagnetic iron oxide NPs are coated with reversibly adsorbing dextran that allows water to readily exchange also in close proximity to the iron oxide surface (Fig. 12.1a). However, stabilization of NPs with low M_w dispersants at high dispersant packing density reduces the accessibility of water molecules to the core surface. The anchor region might be dense and not sufficiently polar to allow direct contact of water molecules with the surface of iron oxide; this reduces the r_1 contrast of NPs stabilized with irreversibly bound dispersants [45] compared to NPs with a physisorbed dextran coating.

Increasing the size of iron oxide NPs increases r_2 [151, 152]. Furthermore, agglomeration and controlled cross-linking [153] have also been shown to increase r_2 [154, 155]. This was confirmed by Monte Carlo simulations [156, 157]. Thus, r_2 of individually stabilized superparamagnetic iron oxide NPs is lower than for NPs stabilized with a physisorbed dextran coating. However, low M_w dispersants that are firmly bound to the iron oxide NP surface through suitable anchors allow independent tuning of the diameter of the core and the thickness of the shell. This creates the possibility to increase r_2 without sacrificing the stability of iron oxide NPs, by increasing the size of the core up to the limit ($>$10 nm) where iron oxide NPs become ferromagnetic. Therefore, individually stabilized superparamagnetic iron oxide NPs [45] can have r_2 values comparable to those of commercially available iron oxide-based MR contrast agents [14, 15] while the former have a hydrodynamic diameter many times smaller than the commercially available analogues.

The influence of the spacer region on the relaxivity is still debated [158, 159]. The hydrophilicity of the polymer shell was shown to influence r_2 values [159]. In the same study r_2 did not change systematically with the thickness of the shell of

superparamagnetic iron oxide NPs [159]. By contrast, r_2 was shown to decrease with shell thickness for NPs stabilized with PEG-based dispersants with molecular weights lower than 1 kDa in another study [158], whereas NPs stabilized with PEG dispersants with M_ws between 1 and 5 kDa had similar relaxivities. A caveat in comparing these studies is that it is questionable whether PEG spacers with $M_w < 1$ kDa result in stable NPs [70]. Thus, the dependence of r_2 on the thickness of the dispersant shell likely was affected by aggregation of NPs for dispersants with low molecular weights.

Specific Adsorption Rate (SAR)

The specific adsorption rate (SAR) determines how effectively NPs generate heat if they are exposed to an alternating magnetic field (AMF). The SAR is the most important property for the use of superparamagnetic iron oxide NPs in hyperthermia treatment or for triggering release of cargo encapsulated in thermoresponsive drug delivery vehicles [57].

For superparamagnetic NPs that have small magnetic anisotropies, the SAR at a fixed frequency ν is proportional to the relaxation time τ of the NPs [57]. This relaxation time increases with increasing size of the core of NPs [160]; Thus, also the SAR increases with increasing size of NPs up to a critical diameter of the core d_{crit}. If $\tau > (2\pi\nu)^{-1}$, the Néel and/or Brownian relaxations of NPs cannot follow the alternating magnetic field and thus the SAR then rapidly decays with increasing τ and therefore size of NPs [57, 160].

The agglomeration of iron oxide NPs is known to increase the magnetic interparticle interactions [161]; this decreases Néel relaxation losses at frequencies typically used for SAR applications [162]. Thus, steric stabilization of individual iron oxide cores increases the SAR, as was experimentally shown on agglomerated and with poly(methyl methacrylate) (PMMA) stabilized superparamagnetic iron oxide NPs [162].

Surface Presentation of Ligands

Different types of untargeted superparamagnetic iron oxide NPs stabilized with weakly adsorbing high M_w dispersants, such as dextran, are FDA approved and used mainly as negative MR contrast agents to detect lesions in the liver and spleen [57]. Adding functional groups to the shell of NPs allows targeting in vitro and in vivo. Potential functional groups suited for targeting in biomedical applications are antibodies [163], peptides [79, 164–166], aptamers [167], DNA [153, 168] and RNA [169] sequences.

Reports where in vivo targeting of superparamagnetic iron oxide NPs is claimed are numerous. However, the vast majority of iron oxide NPs were targeted towards the liver, kidney or lymph nodes, locations they naturally end up during clearance [170]. Alternatively, iron oxide NPs were targeted to tumors and cancer

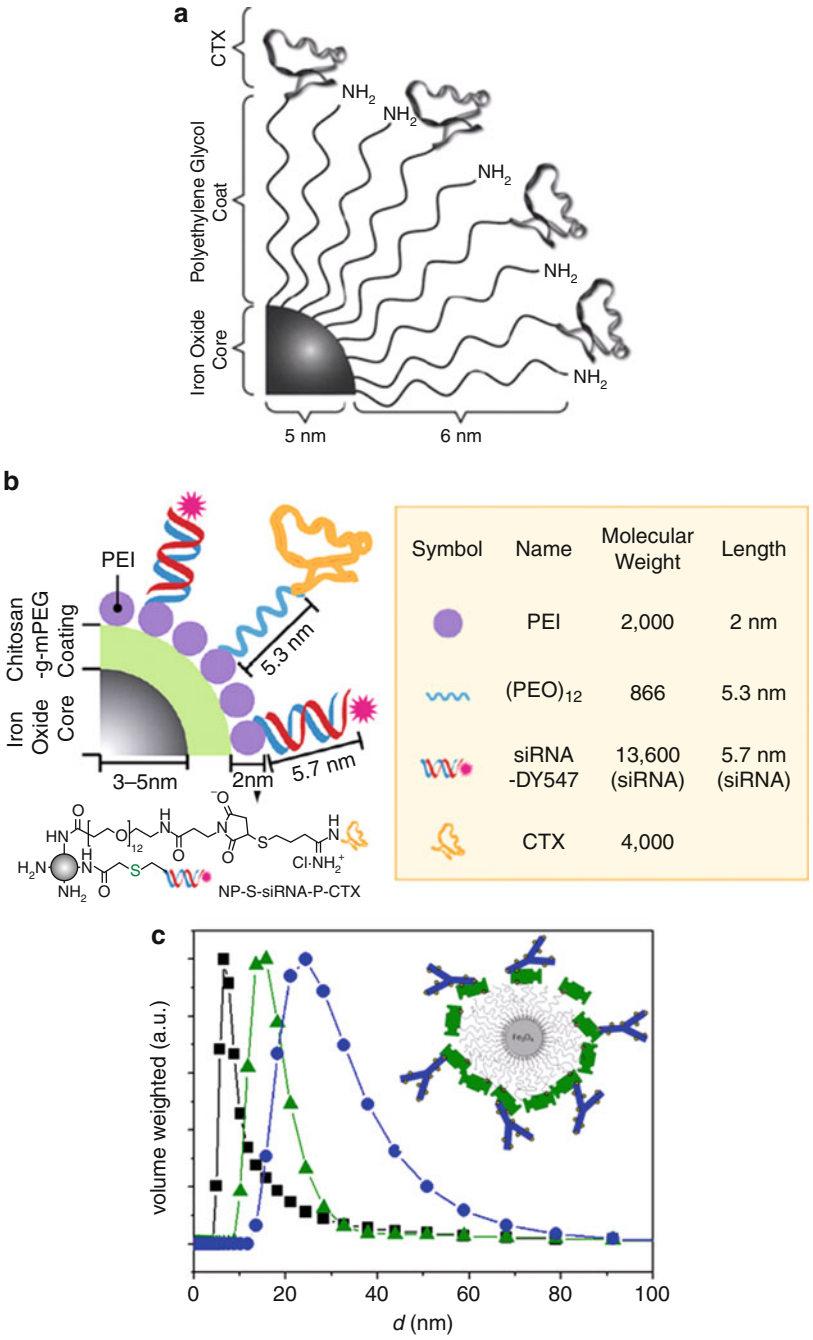

Fig. 12.5 Effect of functionalization on the size of superparamagnetic iron oxide NPs. (**a**) The dispersant shell consisting of amine terminated PEG-silanes [79] (Copyright Wiley-VCH Verlag

cells, where they naturally accumulate due to the enhanced permeation retention (EPR) effect [57, 171]. Proving specific targeting to such organs is therefore difficult as increased accumulation can occur also without specific binding to a target.

The targeting functionality has to be irreversible bound to the particle surface and accessible for binding; this requires covalent coupling to an irreversibly bound dispersant shell. Desorbed targeting ligands can block receptors before functionalized NPs reach these locations. In addition, loss of targeting moieties renders particles unable to bind. The density of ligands presented at the surface of NPs can be closely controlled if NPs are stabilized with low M_w dispersants; this is achieved by co-adsorbing functionalized and unfunctionalized dispersants to the NP surface [21]. By contrast, the serpentine, constantly changing conformation of physisorbed high M_w dispersants prevents efficient addition and controlled presentation of ligands at the interface of NPs [172].

Stealth properties are preserved best if the number of proteins in the ligand shell is minimized. This can be achieved by covalently linking ligands directly to the stealth PEG dispersant shell at a controlled density. Superparamagnetic iron oxide NPs functionalized with covalently bound ligands have typically been coated with dispersants such as dextran that lack well-defined anchors [163]; this renders a controlled surface presentation of functionalities difficult [166].

By contrast, a controlled presentation of ligands at the interface of NPs is possible if they are stabilized with low M_w dispersants such as PEG-silanes (Fig. 12.5a). This was demonstrated on iron oxide NPs functionalized with chlorotoxin [9, 79]. Their performance and uptake was subsequently studied in vitro in cell assays. A controlled surface presentation of ligands is thought to increase the targeting efficiency by decreasing the risk that ligands are buried in the dispersant shell. Furthermore, it allows for closer control over the hydrodynamic diameter of NPs upon functionalization and enables optimization of the number of ligands bound to one NP. The latter is important to ensure sufficient binding affinity while minimizing nonspecific interactions.

Because the hydrodynamic size of superparamagnetic iron oxide NPs significantly influences their uptake by cells [173], control over their hydrodynamic diameter upon functionalization is crucial. Ligands, such as antibodies and peptides are often comparable in size to the iron oxide NPs [169]. Their coupling can therefore significantly change the hydrodynamic size (Fig. 12.5).

Fig. 12.5 (continued) GmbH & Co. KGaA. Reproduced with permission) can be of comparable size to the iron oxide core. The hydrodynamic diameter of sterically stabilized NPs is therefore considerably larger than the size of the core. (**b**) Targeting ligands such as chlorotoxin, siRNA, and fluorophores can have a similar size to that of iron oxide cores. Therefore, the hydrodynamic radius of functionalized NPs can be significantly larger than that of unfunctionalized counterparts [169]. (Biomaterials by Biological Engineering Society. Reproduced with permission of PERGAMON in the format Journal via Copyright Clearance Center). (**c**) The increase in hydrodynamic diameter of iron oxide NPs upon coupling ligands to the dispersant shell is experimentally shown on superparamagnetic iron oxide NPs stabilized with PEG (5 kDa)-nitroDOPA that were further functionalized with neutravidin (*green*) followed by biotinylated antibodies (*blue*)

Ligands can also cross-link and cluster individually stabilized NPs if they carry multiple chemically reactive groups per NP (Fig. 12.5c); this significantly increases the hydrodynamic diameter and prevents elucidation of the effect of ligands on the biodistribution and clearance of functionalized NPs. Therefore, it is of highest importance to measure the hydrodynamic diameter and zeta potential of NPs before and after ligands are coupled to their shells. Differences in the biodistribution and clearance rate of NPs can only be unequivocally attributed to a targeting effect if the size and surface charge of NPs are not significantly altered by the attachment of ligands. Such careful studies were performed to demonstrate in vitro the specific binding of cRGD-functionalized iron oxide NPs to cancer cells [174].

An alternative very good way to elucidate binding specificity of NPs is to functionalize them with different peptide sequences of similar sizes and charges. A comparison of the binding of NPs functionalized with native and scrambled RGD sequences to cells allows assessment of the binding specificity of such NPs [164]. Superparamagnetic iron oxide NPs have most frequently been functionalized with peptides, since the small size of these ligands and the possibility to synthesize them offers easy and cost-effective functionalization. By contrast, only a few antibodies would be able to decorate a NP surface due to steric constraints. It has been shown that multivalent binding greatly enhances the targeting ability of NPs [165]. For this reason, and due to the reduced circulation time of antibody functionalized NPs, peptide and other low M_w molecules might be more promising targeting ligands for superparamagnetic iron oxide NPs than antibodies are [165].

It is important to thoroughly remove excess material after stabilization and functionalization of NPs since the excessive material will comprise biopolymers of similar size as the NPs. Rigorous purification is crucial but difficult to perform if the ligand shell is physisorbed and not cross-linked, as such NPs do not pass column purification and can be damaged by filtration and centrifuge purification. The need to pay attention to the difficulty to completely remove even the smallest ligands was exemplified in a study in which non-complexed ^{64}Cu could not be removed by centrifugation but required purification of iron oxide NPs by column separation [175].

Conclusions

The increasingly demanding and versatile requirements imposed on superparamagnetic iron oxide NPs intended for biomedical applications require close control over the size, structure and surface properties of NPs. The key requirement is colloidal stability under physiological conditions which can only be met if iron oxide NPs are sterically stabilized with dispersants that firmly and for practical purposes irreversibly bind to the surface of the NPs. Dispersants consisting of a suitable anchor covalently linked to a spacer have been shown to meet this stringent requirement.

Close control over the assembly of dispersants at the NP surface allows tuning of the size of the core and thickness of the shell independently. While the magnetic response of superparamagnetic iron oxide NPs is directly related to the size of the core, the stability of NPs and their biodistribution are controlled by the thickness, structure and properties of the shell. Thus, within the limit of superparamagnetic cores, magnetic response of individually stabilized iron oxide NPs can be maximized by increasing the size of the core without compromising their stability. This, however, is only possible if iron oxide NPs are stabilized with optimized dispersants that consist of an irreversibly binding anchor covalently linked to a spacer long enough to provide good steric stability but still small enough to allow high packing densities of dispersants at a sufficient distance from the surface of the core. If these requirements are fulfilled, individually stabilized superparamagnetic iron oxide NPs can be used as highly stable, well-dispersed NPs for a multitude of biomedical applications. End-grafted and irreversibly bound dispersants further allow for controlled functionalization of individually stabilized NPs. This is achieved by simply adjusting the molar ratio of differently functionalized and unfunctionalized dispersants that are grafted to the surface of iron oxide NPs.

In summary, the emerging modular approach to design iron oxide NPs greatly enhances the versatility of iron oxide NP platforms being developed for various biomedical applications. However, ensuring the effect of each functionalization step in this modular approach requires the application of a wide range of characterization techniques from multiple research fields. This inter-disciplinary expertise often is not accessible within one group or even one research environment and is therefore seldom performed in the study of a single NP material. Despite this challenge it is clear that the research and application of iron oxide core-shell NPs is approaching a state of maturity in the understanding of what characterization techniques and material parameters are of importance. We should therefore expect further breakthrough developments in the design of NPs for biomedical and other applications in the near future.

References

1. Lewin M, Carlesso N, Tung CH et al (2000) Tat peptide-derivatized magnetic nanoparticles allow in vivo tracking and recovery of progenitor cells. Nat Biotechnol 18:410–414
2. Pittet MJ, Swirski FK, Reynolds F et al (2006) Labeling of immune cells for in vivo imaging using magnetofluorescent nanoparticles. Nat Protoc 1:73–79
3. Wang DS, He JB, Rosenzweig N et al (2004) Superparamagnetic Fe2O3 Beads-CdSe/ZnS quantum dots core-shell nanocomposite particles for cell separation. Nano Lett 4:409–413
4. Halbreich A, Roger J, Pons JN et al (1998) Biomedical applications of maghemite ferrofluid. Biochimie 80:379–390
5. Pankhurst QA, Thanh NKT, Jones SK et al (2009) Progress in applications of magnetic nanoparticles in biomedicine. J Phys D-Appl Phys 42
6. Namdeo M, Saxena S, Tankhiwale R et al (2008) Magnetic nanoparticles for drug delivery applications. J Nanosci Nanotechnol 8:3247–3271
7. Weissleder R, Hahn PF, Stark DD et al (1987) MR imaging of splenic metastases – ferrite-enhanced detection in rats. Am J Roentgenol 149:723–726

8. Weissleder R, Elizondo G, Wittenberg J et al (1990) Ultrasmall superparamagnetic iron-oxide – characterization of a new class of contrast agents for Mr imaging. Radiology 175:489–493
9. McCarthy JR, Weissleder R (2008) Multifunctional magnetic nanoparticles for targeted imaging and therapy. Adv Drug Deliv Rev 60:1241–1251
10. Hutten A, Sudfeld D, Ennen I et al (2004) New magnetic nanoparticles for biotechnology. J Biotechnol 112:47–63
11. Duran JDG, Arias JL, Gallardo V et al (2008) Magnetic colloids as drug vehicles. J Pharm Sci 97:2948–2983
12. Krishnan KM (2010) Biomedical nanomagnetics: a spin through possibilities in imaging, diagnostics, and therapy. IEEE Trans Magn 46:2523–2558
13. Louie A (2010) Multimodality imaging probes: design and challenges. Chem Rev 110:3146–3195
14. Wang YXJ, Hussain SM, Krestin GP (2001) Superparamagnetic iron oxide contrast agents: physicochemical characteristics and applications in MR imaging. Eur Radiol 11:2319–2331
15. Jung CW, Jacobs P (1995) Physical and chemical-properties of superparamagnetic iron-oxide Mr contrast agents – ferumoxides, ferumoxtran, ferumoxsil. Magn Reson Imaging 13:661–674
16. Lin MM, Kim DK, El Haj AJ et al (2008) Development of Superparamagnetic Iron Oxide Nanoparticles (SPIONS) for translation to clinical applications. IEEE Trans Nanobioscience 7:298–305
17. Cengelli F, Maysinger D, Tschudi-Monnet F et al (2006) Interaction of functionalized superparamagnetic iron oxide nanoparticles with brain structures. J Pharmacol Exp Ther 318:108–116
18. Pardoe H, Chua-anusorn W, St Pierre TG et al (2001) Structural and magnetic properties of nanoscale iron oxide particles synthesized in the presence of dextran or polyvinyl alcohol. J Magn Magn Mater 225:41–46
19. Bautista MC, Bomati-Miguel O, Zhao X et al (2004) Comparative study of ferrofluids based on dextran-coated iron oxide and metal nanoparticles for contrast agents in magnetic resonance imaging. Nanotechnology 15:S154–S159
20. Basiruddin SK, Saha A, Pradhan N et al (2010) Advances in coating chemistry in deriving soluble functional nanoparticle. J Phys Chem C 114:11009–11017
21. Amstad E, Gillich T, Bilecka I et al (2009) Ultrastable iron oxide nanoparticle colloidal suspensions using dispersants with catechol-derived anchor groups. Nano Lett 9:4042–4048
22. Lu AH, Salabas EL, Schuth F (2007) Magnetic nanoparticles: synthesis, protection, functionalization, and application. Angew Chem Int Ed 46:1222–1244
23. Jun YW, Lee JH, Cheon J (2008) Chemical design of nanoparticle probes for high-performance magnetic resonance imaging. Angew Chem Int Ed 47:5122–5135
24. Sun SH, Zeng H, Robinson DB et al (2004) Monodisperse MFe2O4 (M = Fe, Co, Mn) nanoparticles. J Am Chem Soc 126:273–279
25. Thunemann AF, Rolf S, Knappe P et al (2009) In situ analysis of a bimodal size distribution of superparamagnetic nanoparticles. Anal Chem 81:296–301
26. Bonini M, Wiedemann A, Baglioni P (2006) Synthesis and characterization of magnetic nanoparticles coated with a uniform silica shell. Mater Sci Eng C-Biomim Supramol Syst 26:745–750
27. Butter K, Hoell A, Wiedenmann A et al (2004) Small-angle neutron and X-ray scattering of dispersions of oleic-acid-coated magnetic iron particles. J Appl Crystallogr 37:847–856
28. Degen P, Shukla A, Boetcher U et al (2008) Self-assembled ultra-thin coatings of octadecyltrichlorosilane (OTS) formed at the surface of iron oxide nanoparticles. Colloid Polym Sci 286:159–168
29. Cowles RJH (1999) Particle characterization for oil sand processing – 1: particle size measurements using a disc centrifuge. Pet Sci Technol 17:429–442

30. Roonasi P, Holmgren A (2009) A Fourier transform infrared (FTIR) and thermogravimetric analysis (TGA) study of oleate adsorbed on magnetite nano-particle surface. Appl Surf Sci 255:5891–5895
31. Chen S, Li Y, Guo C et al (2007) Temperature-responsive magnetite/PEO-PPO-PEO block copolymer nanoparticles for controlled drug targeting delivery. Langmuir 23:12669–12676
32. Zackrisson M, Stradner A, Schurtenberger P et al (2005) Small-angle neutron scattering on a core-shell colloidal system: a contrast-variation study. Langmuir 21:10835–10845
33. Dingenouts N, Seelenmeyer S, Deike I et al (2001) Analysis of thermosensitive core-shell colloids by small-angle neutron scattering including contrast variation. Phys Chem Chem Phys 3:1169–1174
34. Gelbrich T, Feyen M, Schmidt AM (2006) Magnetic thermoresponsive core-shell nanoparticles. Macromolecules 39:3469–3472
35. Mondini S, Ferretti AM, Puglisi A et al (2012) PEBBLES and PEBBLEJUGGLER: software for accurate, unbiased, and fast measurement and analysis of nanoparticle morphology from transmission electron microscopy (TEM) micrographs. Nanoscale 4:5356–5372
36. Zakharov P, Bhat S, Schurtenberger P et al (2006) Multiple-scattering suppression in dynamic light scattering based on a digital camera detection scheme. Appl Optics 45:1756–1764
37. Scheffold F, Mason TG (2009) Scattering from highly packed disordered colloids. J Phys Condens Matter 21:332102
38. Zhang QA, Thompson MS, Carmichael-Baranauskas AY et al (2007) Aqueous dispersions of magnetite nanoparticles complexed with copolyether dispersants: experiments and theory. Langmuir 23:6927–6936
39. Mefford OT, Vadala ML, Goff JD et al (2008) Stability of polydimethylsiloxane-magnetite nanoparticle dispersions against flocculation: interparticle interactions of polydisperse materials. Langmuir 24:5060–5069
40. Bevan MA, Petris SN, Chan DYC (2002) Solvent quality dependent continuum van der Waals attraction and phase behavior for colloids bearing nonuniform adsorbed polymer layers. Langmuir 18:7845–7852
41. Thanh NTK, Green LAW (2010) Functionalisation of nanoparticles for biomedical applications. Nano Today 5:213–230
42. Verma A, Stellacci F (2010) Effect of surface properties on nanoparticle-cell interactions. Small 6:12–21
43. Xiao ZP, Yang KM, Liang H et al (2010) Synthesis of magnetic, reactive, and thermoresponsive Fe3O4 nanoparticles via surface-initiated RAFT copolymerization of *N*-isopropylacrylamide and acrolein. J Polym Sci Part a-Polym Chem 48:542–550
44. Somaskandan K, Veres T, Niewczas M et al (2008) Surface protected and modified iron based core-shell nanoparticles for biological applications. New J Chem 32:201–209
45. Amstad E, Starmans LWE, Visbal MA et al Influence of the PEG Shell on the stability and magnetic properties of iron oxide nanoparticles (in preparation)
46. Gamarra LF, Amaro E, Alves S et al (2010) Characterization of the biocompatible magnetic colloid on the basis of Fe_3O_4 nanoparticles coated with dextran, used as contrast agent in magnetic resonance imaging. J Nanosci Nanotechnol 10:4145–4153
47. Ma HL, Qi XT, Maitani Y et al (2007) Preparation and characterization of superparamagnetic iron oxide nanoparticles stabilized by alginate. Int J Pharm 333:177–186
48. Park JH, Im KH, Lee SH et al (2005) Preparation and characterization of magnetic chitosan particles for hyperthermia application. J Magn Magn Mater 293:328–333
49. Mahmoudi M, Simchi A, Milani AS et al (2009) Cell toxicity of superparamagnetic iron oxide nanoparticles. J Colloid Interface Sci 336:510–518
50. Chastellain A, Petri A, Hofmann H (2004) Particle size investigations of a multistep synthesis of PVA coated superparamagnetic nanoparticles. J Colloid Interface Sci 278:353–360

51. Schopf B, Neuberger T, Schulze K et al (2005) Methodology description for detection of cellular uptake of PVA coated superparamagnetic iron oxide nanoparticles (SPION) in synovial cells of sheep. J Magn Magn Mater 293:411–418
52. Santra S, Kaittanis C, Grimm J et al (2009) Drug/dye-loaded, multifunctional iron oxide nanoparticles for combined targeted cancer therapy and dual optical/magnetic resonance imaging. Small 5:1862–1868
53. Thunemann AF, Schutt D, Kaufner L et al (2006) Maghemite nanoparticles protectively coated with poly(ethylene imine) and poly(ethylene oxide)-block-poly(glutamic acid). Langmuir 22:2351–2357
54. Shubayev VI, Pisanic TR, Jin SH (2009) Magnetic nanoparticles for theragnostics. Adv Drug Deliv Rev 61:467–477
55. Mosqueira VCF, Legrand P, Morgat JL et al (2001) Biodistribution of long-circulating PEG-grafted nanocapsules in mice: effects of PEG chain length and density. Pharm Res 18:1411–1419
56. Josephson L, Tung CH, Moore A et al (1999) High-efficiency intracellular magnetic labeling with novel superparamagnetic-tat peptide conjugates. Bioconjug Chem 10:186–191
57. Laurent S, Forge D, Port M et al (2008) Magnetic iron oxide nanoparticles: synthesis, stabilization, vectorization, physicochemical characterizations, and biological applications. Chem Rev 108:2064–2110
58. Corot C, Robert P, Idee JM et al (2006) Recent advances in iron oxide nanocrystal technology for medical imaging. Adv Drug Deliv Rev 58:1471–1504
59. Du BY, Mei AX, Tao PJ et al (2009) Poly[*N*-isopropylacrylamide-Co-3-(trimethoxysilyl)-propylmethacrylate] coated aqueous dispersed thermosensitive Fe_3O_4 nanoparticles. J Phys Chem C 113:10090–10096
60. Wang SX, Zhou Y, Guan W et al (2008) One-step copolymerization modified magnetic nanoparticles via surface chain transfer free radical polymerization. Appl Surf Sci 254:5170–5174
61. Zhao B, Brittain WJ (2000) Polymer brushes: surface-immobilized macromolecules. Prog Polym Sci 25:677–710
62. Bae KH, Kim YB, Lee Y et al (2010) Bioinspired synthesis and characterization of gadolinium-labeled magnetite nanoparticles for dual contrast T-1- and T-2-weighted magnetic resonance imaging. Bioconjug Chem 21:505–512
63. Nagase K, Kobayashi J, Okano T (2009) Temperature-responsive intelligent interfaces for biomolecular separation and cell sheet engineering. J R Soc Interface 6:S293–S309
64. Knoll W, Advincula RC (eds) (2011) Functional polymer films, vol 2. Wiley-VCH, Weinheim, Germany
65. Xie J, Xu CJ, Xu ZC et al (2006) Linking hydrophilic macromolecules to monodisperse magnetite (Fe_3O_4) nanoparticles via trichloro-*s*-triazine. Chem Mater 18:5401–5403
66. Xie J, Chen K, Lee H-Y et al (2008) Ultrasmall c(RGDyK)-coated Fe_3O_4 nanoparticles and their specific targeting to integrin alpha(v)beta3-rich tumor cells. J Am Chem Soc 130:7542–7543
67. Xu CJ, Xu KM, Gu HW et al (2004) Dopamine as a robust anchor to immobilize functional molecules on the iron oxide shell of magnetic nanoparticles. J Am Chem Soc 126:9938–9939
68. Gu HW, Yang ZM, Gao JH et al (2005) Heterodimers of nanoparticles: formation at a liquid-liquid interface and particle-specific surface modification by functional molecules. J Am Chem Soc 127:34–35
69. Amstad E, Isa L, Reimhult E (2011) Nitrocatechol dispersants to tailor superparamagnetic Fe_3O_4 nanoparticles. Chimia 64:826
70. Isa L, Amstad E, Textor M et al (2010) Self-assembly of iron oxide-poly(ethylene glycol) core-shell nanoparticles at liquid-liquid interfaces. Chimia 64:145–149
71. Yu S, Chow GM (2004) Carboxyl group (-CO_2H) functionalized ferrimagnetic iron oxide nanoparticles for potential bio-applications. J Mater Chem 14:2781–2786

72. White MA, Johnson JA, Koberstein JT et al (2006) Toward the syntheses of universal ligands for metal oxide surfaces: controlling surface functionality through click chemistry. J Am Chem Soc 128:11356–11357
73. Song HT, Choi JS, Huh YM et al (2005) Surface modulation of magnetic nanocrystals in the development of highly efficient magnetic resonance probes for intracellular labeling. J Am Chem Soc 127:9992–9993
74. Basly B, Felder-Flesch D, Perriat P et al (2010) Dendronized iron oxide nanoparticles as contrast agents for MRI. Chem Commun 46:985–987
75. Lalatonne Y, Paris C, Serfaty JM et al (2008) Bis-phosphonates – ultra small superparamagnetic iron oxide nanoparticles: a platform towards diagnosis and therapy. Chem Commun 22:2553–2555
76. Zhou Y, Wang SX, Ding BJ et al (2008) Modification of magnetite nanoparticles via surface-initiated atom transfer radical polymerization (ATRP). Chem Eng J 138:578–585
77. Forge D, Laurent S, Gossuin Y et al (2011) An original route to stabilize and functionalize magnetite nanoparticles for theranosis applications. J Magn Magn Mater 323:410–415
78. Sun CR, Du K, Fang C et al (2010) PEG-mediated synthesis of highly dispersive multifunctional superparamagnetic nanoparticles: their physicochemical properties and function in vivo. Acs Nano 4:2402–2410
79. Veiseh O, Gunn JW, Kievit FM et al (2009) Inhibition of tumor-cell invasion with chlorotoxin-bound superparamagnetic nanoparticles. Small 5:256–264
80. Larsen EKU, Nielsen T, Wittenborn T et al (2009) Size-dependent accumulation of PEGylated Silane-coated magnetic iron oxide nanoparticles in murine tumors. ACS Nano 3:1947–1951
81. Dalsin JL, Lin LJ, Tosatti S et al (2005) Protein resistance of titanium oxide surfaces modified by biologically inspired mPEG-DOPA. Langmuir 21:640–646
82. Corbierre MK, Cameron NS, Lennox RB (2004) Polymer-stabilized gold nanoparticles with high grafting densities. Langmuir 20:2867–2873
83. Kim M, Chen YF, Liu YC et al (2005) Super-stable, high-quality Fe_3O_4 dendron-nanocrystals dispersible in both organic and aqueous solutions. Adv Mater 17:1429
84. Chen ZP, Zhang Y, Xu K et al (2008) Stability of hydrophilic magnetic nanoparticles under biologically relevant conditions. J Nanosci Nanotechnol 8:6260–6265
85. Haensch C, Chiper M, Ulbricht C et al (2008) Reversible supramolecular functionalization of surfaces: terpyridine ligands as versatile building blocks for noncovalent architectures. Langmuir 24:12981–12985
86. Waite JH, Tanzer ML (1981) Polyphenolic substance of mytilus-edulis – novel adhesive containing L-dopa and hydroxyproline. Science 212:1038–1040
87. Lynch MW, Valentine M, Hendrickson DN (1982) Mixed-valence semi-quinone catecholate iron complexes. J Am Chem Soc 104:6982–6989
88. Heistand RH, Roe AL, Que L (1982) Dioxygenase models – crystal-structures of [*N*, *N*′-(1,2-phenylene)bis(salicylideniminato)](catecholato-*O*)iron(III) and Mu-(1,4-benzenediolato-*O*, *O*′)-bis[*N*, *N*′-ethylenebis(salicylideniminato)iron(III)]. Inorg Chem 21:676–681
89. Attia AS, Bhattacharya S, Pierpont CG (1995) Potential for redox isomerism by quinone complexes of Iron(Iii). – studies on complexes of the Fe-III(N-N)(Dbsq)(Dbcat) series with 2,2′-bipyridine and *N*, *N*, *N*′, *N*′-tetramethylethylenediamine coligands. Inorg Chem 34:4427–4433
90. Grillo VA, Hanson GR, Wang DM et al (1996) Synthesis, x-ray structural determination, and magnetic susceptibility, Mossbauer, and EPR studies of (Ph(4)P)(2)[Fe-2(Cat)(4)(H_2O)(2)]·6H(2)O, a catecholato-bridged dimer of iron(III). Inorg Chem 35:3568–3576
91. Girerd JJ, Boillot ML, Blain G et al (2008) An EPR investigation of the electronic structure of pseudo-octahedral and spin crossover catecholato-iron(III) complexes in the low-spin state. Inorg Chim Acta 361:4012–4016

92. Kalyanaraman B, Felix CC, Sealy RC (1985) Semiquinone anion radicals of catechol(amine) S, catechol estrogens, and their metal-ion complexes. Environ Health Perspect 64:185–198
93. Cox DD, Que L (1988) Functional models for catechol 1,2-dioxygenase – the role of the Iron (III) center. J Am Chem Soc 110:8085–8092
94. Emerson JP, Kovaleva EG, Farquhar ER et al (2008) Swapping metals in Fe- and Mn-dependent dioxygenases: evidence for oxygen activation without a change in metal redox state. Proc Natl Acad Sci U S A 105:7347–7352
95. Shultz MD, Reveles JU, Khanna SN et al (2007) Reactive nature of dopamine as a surface functionalization agent in iron oxide nanoparticles. J Am Chem Soc 129:2482–2487
96. Goldmann AS, Schodel C, Walther A et al (2010) Biomimetic mussel adhesive inspired clickable anchors applied to the functionalization of Fe_3O_4 nanoparticles. Macromol Rapid Commun 31:1608–1615
97. Galpin JR, Tielens LGM, Veldink GA et al (1976) Interaction of some catechol derivatives with iron atom of soybean lipoxygenase. FEBS Lett 69:179–182
98. Kawabata T, Schepkin V, Haramaki N et al (1996) Iron coordination by catechol derivative antioxidants. Biochem Pharmacol 51:1569–1577
99. Crisponi G, Remelli M (2008) Iron chelating agents for the treatment of iron overload. Coord Chem Rev 252:1225–1240
100. Nurchi VM, Pivetta T, Lachowicz JI et al (2009) Effect of substituents on complex stability aimed at designing new iron(III) and aluminum(III) chelators. J Inorg Biochem 103:227–236
101. Amstad E, Fischer H, Gehring AU et al (2011) Magnetic decoupling of surface Fe(3+) in magnetite nanoparticles upon Nitrocatechol-anchored dispersant binding. Chem A Eur J 17:7396–7398
102. Amstad E, Gehring AU, Fischer H et al (2011) Influence of electronegative substituents on the binding affinity of catechol-derived anchors to Fe(3)O(4) nanoparticles. J Phys Chem C 115:683–691
103. Fritz G, Schadler V, Willenbacher N et al (2002) Electrosteric stabilization of colloidal dispersions. Langmuir 18:6381–6390
104. Gast AP (1996) Structure, interactions, and dynamics in tethered chain systems. Langmuir 12:4060–4067
105. Witten TA, Pincus PA (1986) Colloid stabilization by long grafted polymers. Macromolecules 19:2509–2513
106. Vincent B, Edwards J, Emmett S et al (1986) Depletion flocculation in dispersions of sterically-stabilized particles (soft spheres). Colloid Surf 18:261–281
107. Degennes PG (1980) Conformations of polymers attached to an interface. Macromolecules 13:1069–1075
108. Milner ST, Witten TA, Cates ME (1988) Theory of the grafted polymer brush. Macromolecules 21:2610–2619
109. Zhulina EB, Borisov OV, Priamitsyn VA (1990) Theory of steric stabilization of colloid dispersions by grafted polymers. J Colloid Interface Sci 137:495–511
110. Shim DFK, Cates ME (1989) Finite extensibility and density saturation effects in the polymer brush. Journal De Physique 50:3535–3551
111. Alexander S (1977) Polymer adsorption on small spheres – scaling approach. Journal De Physique 38:977–981
112. Birshtein TM, Zhulina EB (1984) Conformations of star-branched macromolecules. Polymer 25:1453–1461
113. Dan N, Tirrell M (1992) Polymers tethered to curved interfaces – a self-consistent-field analysis. Macromolecules 25:2890–2895
114. Ball RC, Marko JF, Milner ST et al (1991) Polymers grafted to a convex surface. Macromolecules 24:693–703
115. Toral R, Chakrabarti A (1993) Monte-Carlo study of polymer-chains end-grafted onto a spherical interface. Phys Rev E 47:4240–4246

116. Li H, Witten TA (1994) Polymers grafted to convex surfaces – a variational approach. Macromolecules 27:449–457
117. Martin JI, Wang ZG (1995) Polymer brushes – scaling, compression forces, interbrush penetration, and solvent size effects. J Phys Chem 99:2833–2844
118. Lin EK, Gast AP (1996) Self consistent field calculations of interactions between chains tethered to spherical interfaces. Macromolecules 29:390–397
119. Lo Verso F, Egorov SA, Milchev A et al (2010) Spherical polymer brushes under good solvent conditions: molecular dynamics results compared to density functional theory. J Chem Phys 133:184901
120. Lo Verso F, Yelash L, Egorov SA et al (2011) Interactions between polymer brush-coated spherical nanoparticles: the good solvent case. J Chem Phys 135:214902
121. Gillich T, Acikgoz C, Isa L et al (2013) PEG-stabilized core-shell nanoparticles: impact of linear versus dendritic polymer shell architecture on colloidal properties and the reversibility of temperature-induced aggregation. ACS Nano 7:316–329
122. Isa L, Calzolari DCE, Pontoni D et al (2013) Core-shell nanoparticle monolayers at planar liquid-liquid interfaces: effects of polymer architecture on the interface microstructure. Soft Matter 9:3789–3797
123. Owens DE, Peppas NA (2006) Opsonization, biodistribution, and pharmacokinetics of polymeric nanoparticles. Int J Pharm 307:93–102
124. Jeon SI, Lee JH, Andrade JD et al (1991) Protein surface interactions in the presence of polyethylene oxide 1. Simplified theory. J Colloid Interface Sci 142:149–158
125. Bhat R, Timasheff SN (1992) Steric exclusion is the principal source of the preferential hydration of proteins in the presence of polyethylene glycols. Protein Sci 1:1133–1143
126. Feldman K, Hahner G, Spencer ND et al (1999) Probing resistance to protein adsorption of oligo(ethylene glycol)-terminated self-assembled monolayers by scanning force microscopy. J Am Chem Soc 121:10134–10141
127. Wang RLC, Kreuzer HJ, Grunze M (1997) Molecular conformation and solvation of oligo (ethylene glycol)-terminated self-assembled monolayers and their resistance to protein adsorption. J Phys Chem B 101:9767–9773
128. Roosjen A, de Vries J, van der Mei HC et al (2005) Stability and effectiveness against bacterial adhesion of poly(ethylene oxide) coatings in biological fluids. J Biomed Mater Res B Appl Biomater 73B:347–354
129. Shen MC, Martinson L, Wagner MS et al (2002) PEO-like plasma polymerized tetraglyme surface interactions with leukocytes and proteins: in vitro and in vivo studies. J Biomater Sci Polym Ed 13:367–390
130. Konradi R, Pidhatika B, Muhlebach A et al (2008) Poly-2-methyl-2-oxazoline: a peptide-like polymer for protein-repellent surfaces. Langmuir 24:613–616
131. Pasche S, De Paul SM, Voros J et al (2003) Poly(L-lysine)-graft-poly(ethylene glycol) assembled monolayers on niobium oxide surfaces: a quantitative study of the influence of polymer interfacial architecture on resistance to protein adsorption by ToF-SIMS and in situ OWLS. Langmuir 19:9216–9225
132. Michel R, Pasche S, Textor M et al (2005) Influence of PEG architecture on protein adsorption and conformation. Langmuir 21:12327–12332
133. Szleifer I (1997) Protein adsorption on surfaces with grafted polymers: a theoretical approach. Biophys J 72:595–612
134. Zahr AS, Davis CA, Pishko MV (2006) Macrophage uptake of core-shell nanoparticles surface modified with poly(ethylene glycol). Langmuir 22:8178–8185
135. Gessner A, Paulke BR, Muller RH et al (2006) Protein rejecting properties of PEG-grafted nanoparticles: Influence of PEG-chain length and surface density evaluated by two-dimensional electrophoresis and bicinchoninic acid (BCA)-proteinassay. Pharmazie 61:293–297

136. Kenworthy AK, Hristova K, Needham D et al (1995) Range and magnitude of the steric pressure between bilayers containing phospholipids with covalently attached Poly(ethylene glycol). Biophys J 68:1921–1936
137. Vittaz M, Bazile D, Spenlehauer G et al (1996) Effect of PEO surface density on long-circulating PLA-PEO nanoparticles which are very low complement activators. Biomaterials 17:1575–1581
138. Storm G, Belliot SO, Daemen T et al (1995) Surface modification of nanoparticles to oppose uptake by the mononuclear phagocyte system. Adv Drug Deliv Rev 17:31–48
139. Klibanov AL, Maruyama K, Torchilin VP et al (1990) Amphipathic polyethyleneglycols effectively prolong the circulation time of liposomes. FEBS Lett 268:235–237
140. Mori A, Klibanov AL, Torchilin VP et al (1991) Influence of the steric barrier activity of amphipathic poly(ethyleneglycol) and ganglioside GM1 on the circulation time of liposomes and on the target binding of immunoliposomes invivo. FEBS Lett 284:263–266
141. Decuzzi P, Pasqualini R, Arap W et al (2009) Intravascular delivery of particulate systems: does geometry really matter? Pharm Res 26:235–243
142. Dobrovolskaia MA, McNeil SE (2007) Immunological properties of engineered nanomaterials. Nat Nanotechnol 2:469–478
143. Gbadamosi JK, Hunter AC, Moghimi SM (2002) PEGylation of microspheres generates a heterogeneous population of particles with differential surface characteristics and biological performance. FEBS Lett 532:338–344
144. Tiefenauer LX, Tschirky A, Kuhne G et al (1996) In vivo evaluation of magnetite nanoparticles for use as a tumor contrast agent in MRI. Magn Reson Imaging 14:391–402
145. Harper GR, Davies MC, Davis SS et al (1991) Steric stabilization of microspheres with grafted polyethylene oxide reduces phagocytosis by rat Kupffer cells-invitro. Biomaterials 12:695–704
146. Lacava LM, Garcia VAP, Kuckelhaus S et al (2004) Long-term retention of dextran-coated magnetite nanoparticles in the liver and spleen. J Magn Magn Mater 272:2434–2435
147. Berkowit A, Schuele WJ, Flanders PJ (1968) Influence of crystallite size on magnetic properties of acicular gamma-Fe_2O_3 particles. J Appl Phys 39:1261
148. Dutta P, Pai S, Seehra MS et al (2009) Size dependence of magnetic parameters and surface disorder in magnetite nanoparticles. J Appl Phys 105:7B501
149. Krycka KL, Booth RA, Hogg CR et al (2010) Core-shell magnetic morphology of structurally uniform magnetite nanoparticles. Phys Rev Lett 104:207203
150. Vidal-Vidal J, Rivas J, Lopez-Quintela MA (2006) Synthesis of monodisperse maghemite nanoparticles by the microemulsion method. Colloid SurfA Physicochem Eng Asp 288:44–51
151. Jun YW, Huh YM, Choi JS et al (2005) Nanoscale size effect of magnetic nanocrystals and their utilization for cancer diagnosis via magnetic resonance imaging. J Am Chem Soc 127:5732–5733
152. Cheon J, Lee JH (2008) Synergistically integrated nanoparticles as multimodal probes for nanobiotechnology. Acc Chem Res 41:1630–1640
153. Josephson L, Perez JM, Weissleder R (2001) Magnetic nanosensors for the detection of oligonucleotide sequences. Angew Chem Int Ed 40:3204–3206
154. Berret JF, Schonbeck N, Gazeau F et al (2006) Controlled clustering of superparamagnetic nanoparticles using block copolymers: design of new contrast agents for magnetic resonance imaging. J Am Chem Soc 128:1755–1761
155. Seo SB, Yang J, Lee TI et al (2008) Enhancement of magnetic resonance contrast effect using ionic magnetic clusters. J Colloid Interface Sci 319:429–434
156. Brown KA, Vassiliou CC, Issadore D et al (2010) Scaling of transverse nuclear magnetic relaxation due to magnetic nanoparticle aggregation. J Magn Magn Mater 322:3122–3126
157. Matsumoto Y, Jasanoff A (2008) T-2 relaxation induced by clusters of superparamagnetic nanoparticles: Monte Carlo simulations. Magn Reson Imaging 26:994–998

158. LaConte LEW, Nitin N, Zurkiya O et al (2007) Coating thickness of magnetic iron oxide nanoparticles affects R-2 relaxivity. J Magn Reson Imaging 26:1634–1641
159. Duan HW, Kuang M, Wang XX et al (2008) Reexamining the effects of particle size and surface chemistry on the magnetic properties of iron oxide nanocrystals: new insights into spin disorder and proton relaxivity. J Phys Chem C 112:8127–8131
160. Rosensweig RE (2002) Heating magnetic fluid with alternating magnetic field. J Magn Magn Mater 252:370–374
161. Buscher K, Helm CA, Gross C et al (2004) Nanoparticle composition of a ferrofluid and its effects on the magnetic properties. Langmuir 20:2435–2444
162. Rovers SA, Dietz C, van der Poel LAM et al (2010) Influence of distribution on the heating of superparamagnetic iron oxide nanoparticles in Poly(methyl methacrylate) in an alternating magnetic field. J Phys Chem C 114:8144–8149
163. Tsourkas A, Shinde-Patil VR, Kelly KA et al (2005) In vivo imaging of activated endothelium using an anti-VCAM-1 magnetooptical probe. Bioconjug Chem 16:576–581
164. Kelly KA, Allport JR, Tsourkas A et al (2005) Detection of vascular adhesion molecule-1 expression using a novel multimodal nanoparticle. Circ Res 96:327–336
165. Montet X, Funovics M, Montet-Abou K et al (2006) Multivalent effects of RGD peptides obtained by nanoparticle display. J Med Chem 49:6087–6093
166. Martin AL, Hickey JL, Ablack AL et al (2010) Synthesis of bombesin-functionalized iron oxide nanoparticles and their specific uptake in prostate cancer cells. J Nanopart Res 12:1599–1608
167. Yigit MV, Mazumdar D, Kim HK et al (2007) Smart "Turn-on" magnetic resonance contrast agents based on aptamer-functionalized superparamagnetic iron oxide nanoparticles. Chembiochem 8:1675–1678
168. Cutler JI, Zheng D, Xu XY et al (2010) Polyvalent oligonucleotide iron oxide nanoparticle "Click" conjugates. Nano Lett 10:1477–1480
169. Veiseh O, Kievit FM, Fang C et al (2010) Chlorotoxin bound magnetic nanovector tailored for cancer cell targeting, imaging, and siRNA delivery. Biomaterials 31:8032–8042
170. Cho EC, Glaus C, Chen JY et al (2010) Inorganic nanoparticle-based contrast agents for molecular imaging. Trends Mol Med 16:561–573
171. Gindy ME, Prud'homme RK (2009) Multifunctional nanoparticles for imaging, delivery and targeting in cancer therapy. Expert Opin Drug Deliv 6:865–878
172. Sun C, Lee JSH, Zhang MQ (2008) Magnetic nanoparticles in MR imaging and drug delivery. Adv Drug Deliv Rev 60:1252–1265
173. Huang J, Bu LH, Xie J et al (2011) Effects of nanoparticle size on cellular uptake and liver MRI with polyvinylpyrrolidone-coated iron oxide nanoparticles. ACS Nano 4:7151–7160
174. Yu MK, Park J, Jeong YY et al (2010) Integrin-targeting thermally cross-linked superparamagnetic iron oxide nanoparticles for combined cancer imaging and drug delivery. Nanotechnology 21:415102
175. Jarrett BR, Gustafsson B, Kukis DL et al (2008) Synthesis of Cu-64-labeled magnetic nanoparticles for multimodal imaging. Bioconjug Chem 19:1496–1504